Deposition and characterization of $Pb(Zr,Ti)O_3$ sol–gel thin films for piezoelectric cantilever beams

INSTITUTE OF PHYSICS PUBLISHING SMART MATERIALS AND STRUCTURES
Smart Mater. Struct. **16** (2007) 93–99 doi:10.1088/0964-1726/16/1/011

Deposition and characterization of $Pb(Zr, Ti)O_3$ sol–gel thin films for piezoelectric cantilever beams

Mengwei Liu[1], Jing Wang[2], Liding Wang[1] and Tianhong Cui[3]

[1] MST Research Center, Dalian University of Technology, Dalian 116023, People's Republic of China
[2] Department of Electronic Engineering, Dalian University of Technology, Dalian 116023, People's Republic of China
[3] Department of Mechanical Engineering, University of Minnesota, 111 Church Street SE, Minneapolis, MN 55455, USA

E-mail: tcui@me.umn.edu

Received 5 November 2005, in final form 16 September 2006
Published 23 November 2006
Online at stacks.iop.org/SMS/16/93

Abstract
PZT thin films of various thickness were deposited on $Pt(111)/Ti/SiO_2/Si(100)$ substrates by the sol–gel method. A new method to control the crystallographic orientation of the PZT thin films by modifying the coating layers in one annealing cycle is presented in this paper. PZT films with (111) and (100) preferred orientation were obtained using the multi-coating-layer-annealed and the one-coating-layer-annealed sol–gel methods, respectively. The optimized baking and annealing temperatures at 200 and 600 °C were obtained by analyzing the phase transformation of the PZT precursor solution. The effect of film thickness on the microstructures, crystalline phases, and electrical properties of the PZT films was investigated. Compared to the multi-coating-layer-annealed method, the one-coating-layer-annealed method decreases the residual stress of the PZT films. The remanent polarization increases with the thickness of the PZT films. The remanent polarization (P_r) and coercive fields (E_c) of the one-coating-layer-annealed PZT films with 1.6 μm thickness are 25.7 $\mu C\ cm^{-2}$ and 59.2 $kV\ cm^{-1}$, respectively. New microcantilevers with two PZT piezoelectric elements and three electric electrodes were designed. These structures can be applied to microsensors, microactuators, or versatile devices having both sensing and actuating functions. The cantilevers were successfully fabricated with wet and dry combined bulk micromachining technique.

1. Introduction

During recent years, many efforts have been undertaken on the study of microelectromechanical system (MEMS) based on piezoelectric thin-film materials and silicon technology, which include ultrasonic microsensors [1], force sensors for scanning force microscopy [2], accelerometers [3, 4], cantilever actuators [5, 6], ultrasonic micromotors [7], and micropumps [8, 9]. ZnO and PZT thin films are the two primary piezoelectric materials used in microsensor or microactuator applications. More attention has been attracted to PZT film since its piezoelectric constants are an order of magnitude higher than those of ZnO film.

PZT films can be deposited by various methods such as metal–organic chemical vapour deposition (MOCVD) [10], sol–gel [11–13], metal organic decomposition (MOD) [14], hydrothermal method [15], sputtering [16], and pulsed laser deposition (PLD) [17]. Among them, the sol–gel technique is more favorable due to its advantages such as large deposition area, easy composition control, and low cost. The crystallographic orientation is a key factor to affect the electric properties of the PZT films. PZT films

with (100) preferred orientation were found to have the higher piezoelectric constants than films with (111) preferred orientation [13, 18, 19]. Many methods have been used to control the crystallographic orientation of PZT films, such as deposition temperature [20], orientation of the Pt substrate [13, 19, 21], and seed layers beneath the PZT films [18]. In this work, a novel method to control the crystallographic orientation of PZT thin films is presented. PZT films with preferred (111) and (100) orientation were obtained by modifying the coating layers in one annealing cycle of the sol–gel process.

Another important parameter is film thickness of the PZT films. It is reported that the piezoelectric constants of the PZT films increase with the film thickness [12, 13]. However, when the film thickness is larger than a critical value, residual stress-induced cracking of the PZT films on metal electrodes deposited on silicon substrates will occur [22]. In this work, PZT thin films of various thicknesses with different crystallographic orientation were deposited by the five-coating-layer-annealed and one-coating-layer-annealed sol–gel process. The critical thickness of the PZT films prepared by the two annealing process was compared. The effect of film thickness on the microstructures, crystalline phases and electrical properties of the PZT films was investigated.

Many structures have been designed and fabricated for MEMS devices with PZT films, such as accelerometers or ultrasonic microactuators with diaphragm structure [4, 23, 24], trampoline-type accelerometers [4, 25], MEMS sensors or actuators with microcantilever beams [26–32]. There has been much work recently on microcantilevers because of their simple application design, fast response time and easy integration into semiconductor technology. Most piezoelectric microcantilevers have been designed by preparing the PZT thin film sandwiched between two metal electrodes on silicon cantilever structures. We design two novel piezoelectric microcantilevers with PZT piezoelectric elements (two layers or two segments of PZT films) and three electric electrodes. The bimorph and two-segment piezoelectric cantilevers can be used as a microsensor, microactuator, or a versatile device integrating the sensing and actuating functions. This paper presents the successful fabrication of bimorph piezoelectric cantilevers.

2. Deposition and characterization of PZT films

PZT films were deposited by the sol–gel method. Pt(111)/Ti/SiO_2/Si(100) substrates were prepared to deposit PZT films on. A SiO_2 layer of 900 nm was synthesized on n-type (100) Si by dry oxidation at 1180 °C for 1.5 h. Pt/Ti/SiO_2/Si substrates were prepared by sputtering 90 nm of titanium onto the thermally oxidized silicon wafers, and this was followed by sputtering 250 nm of platinum using a radio-frequency (RF) magnetron sputtering system without substrate heating.

Precursor solutions were prepared from lead acetate trihydrate [$Pb(CH_3COO)_2{\cdot}3H_2O$], zirconium nitrate pentahydrate [$Zr(NO_3)_4{\cdot}5H_2O$], and titanium tetrobutoxide [$Ti(O(CH_2)_3CH_3)_4$]. 2-methoxyethanol [$HOCH_2CH_2OCH_3$] and acetylacetone [$CH_3COCH_2COCH_3$] were used as the solvent and the chemical modifier. The Zr/Ti ratio was chosen as 50/50 and 15% excess of lead was added to the precursor solutions to compensate for the loss of lead during the final annealing process. The preparation flow chart of precursor solution of PZT is shown in figure 1.

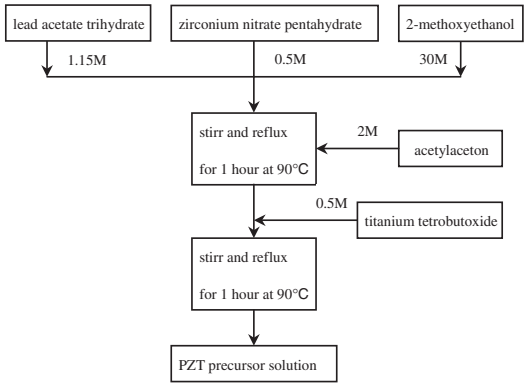

Figure 1. Preparation flow chart of the precursor solution of the PZT films.

The decomposition process of the precursor solution was investigated by thermogravimetric analysis (TGA) and differential thermal analysis (DTA) from 20 to 800 °C in an air ambient with a heating rate of 10 °C min^{-1} (TGA/SDTA 851e, Mettler Toledo, Germany). After the precursor solution was spin-coated on Pt/Ti/SiO_2/Si substrates at 2000 rpm for 30 s, the wet films were heated at 400, 420, 450, 480, 520, 550, and 600 °C, respectively. X-ray diffraction (XRD) was used to examine the phase transformation of PZT materials at different temperatures (XRD-6000, Shimadzu, Japan).

PZT thin films were deposited using a multiple coating and annealing process. Before spin-coating, the precursor solutions were filtered through filter paper to avoid particulate contamination. A spin program with a speed of 4000 rpm for 30 s was used to produce the wet thin films. After each coating, the wet PZT thin film was baked at 200 °C on a hot plate for 5 min. In order to control the crystallographic orientation of the PZT thin films, two annealing processes were used to prepare the PZT films.

(1) Five-coating-layer PZT film was annealed at 600 °C for 30 min in an air atmosphere. In this sol–gel process, five times of spin-coating and pre-baking, and one time of post-annealing composed of a coating and annealing cycle were used. PZT thin films with various thickness were obtained by repeating this cycle for one to four times. We denote these films as PZT-5*1, PZT-5*2, PZT-5*3 and PZT-5*4, respectively.
(2) One-coating-layer PZT film was annealed at 600 °C for 5 min in an air atmosphere. Compared to the above-mentioned sol–gel process, the PZT coating layer in a coating and annealing cycle was decreased from five layers to one layer. Four PZT films with 6, 12, 18, and 24 coating layers were deposited by this sol–gel method, which are denoted as PZT-1*6, PZT-1*12, PZT-1*18 and PZT-1*24.

The surface and cross-section views of the PZT films were observed using a scanning electron microscope (JSM-5600LV, JEOL, Japan). The phases and crystal orientations of PZT films with different thickness were examined by x-ray diffraction.

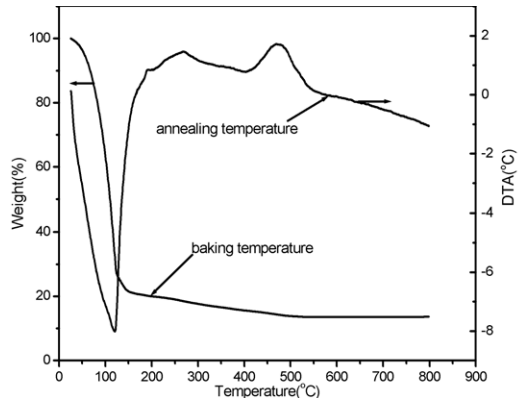

Figure 2. Thermal analysis (DTA and TGA) of PZT 50/50 precursor solution under air atmosphere (heating rate: 10 °C min^{-1}).

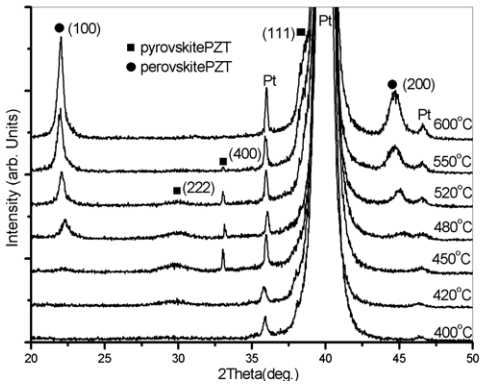

Figure 3. XRD patterns of PZT precursor solution heated to various temperatures.

Polarization–electric field (P–E) loops were measured using a modified Sawyer–Tower circuit with a 100 Hz sine wave.

3. Results and discussion

3.1. Thermal analysis of the precursor solution

Figure 2 shows the thermogravimetric analysis (TGA) and differential thermal analysis (DTA) of the precursor solution. The phase transformation of PZT materials by heating the PZT gel at different temperatures was examined by x-ray diffraction, as shown in figure 3. The DTA curve shows that there is an endothermic reaction from 20 to 170 °C with a peak around 120 °C. By combining with the TGA result, the endothermic event accounted for a major weight loss (80 wt%), 69.3% of the total weight loss in the whole decomposition process from 20 to 800 °C. In our experiment, the firing temperature of the PZT precursor solution was selected at 200 °C because a large weight loss corresponding to the evaporation of water and organic groups is considered to have occurred in this process.

Following this stage, the DTA curve exhibits two exothermic reactions peaks from 170 to 575 °C, and a weight loss of about 6.5 wt% occurred in this temperature range. As shown in XRD patterns (figure 3), the PZT gel heat-treated at 400 °C was amorphous, suggesting that the exothermic event between 170 to 400 °C was not due to phase transformation. Therefore, the exothermic event and the weight loss in this temperature range resulted from the decomposition of organic groups and the formation of metal oxides. From the XRD results, the crystallization of PZT mainly took place above 420 °C, indicating the second exothermic reaction between 400 and 575 °C with small weight loss (∼2 wt%) resulting from the crystallization of pyrochlore phase and perovskite phase. As shown in figure 3, the pyrochlore phase existed in the PZT precursor solution heat-treated between 420 and 550 °C, and it decreased with the increase of heat-treatment temperature. The perovskite phase appeared when the film heated at 480 °C. Although the PZT (111) peak was overlapped with a broad Pt(111) peak, it can be seen that (100)/(111)/(200) mixed texture developed rapidly with the disappearance of pyrochlore phase. The final annealing temperature was selected at 600 °C because a single perovskite phase forms at this temperature.

3.2. Micromorphology of the PZT films

The SEM photographs of the film surfaces reveal that PZT-5*1, PZT-5*2 and PZT-5*3 (with thickness of 280, 560, and 860 nm, respectively) are dense and crack free. No dependence of grain size on film thickness is evident in the SEM photographs. The average grain size of the PZT films is about 200–250 nm. Figure 4 shows the surface and cross-section views of the films undergoing three annealing cycles (PZT-5*3). Cross-sectional SEM photographs indicated that the films with different thickness have well-aligned columnar grains. No interfaces are observed between the three annealing layers identifying the epitaxial growth of PZT grains between various annealing interfaces. As shown in figure 5, residual tensile stresses in PZT films undergoing four annealing cycles (PZT-5*4) caused film cracking. It is indicated that the critical thickness of the PZT films deposited by this annealing process is about 0.86 μm.

SEM views revealed that the four PZT films of PZT-1*6, PZT-1*12, PZT-1*18 and PZT-1*24 (with thickness of 410, 800, 1200 and 1640 nm, respectively) are dense. Compared to the five-coating-layer-annealed method, no difference in the grain size of the PZT films prepared by the one-coating-layer-annealed method was found. However, with the increase of the coating layers, a few hillocks and voids were observed in the surface of the PZT films. No crack was found even in PZT-1*24 (1.64 μm), which indicates that the critical thickness of the PZT films deposited by the one-coating-layer-annealed method is thicker than 1.64 μm. This annealing process apparently decreases the residual stress of the PZT films.

3.3. Phase crystallization of the PZT films

Figure 6 shows the XRD patterns of Pt/Ti/SiO_2/Si substrate and PZT films of PZT-5*1, PZT-5*2 and PZT-5*3. X-ray diffraction indicates that the Pt/Ti/SiO_2/Si substrate grows with a high degree of (111) orientation, and all the PZT films prepared by the five-coating-layer-annealed method consist of the perovskite phase, and exhibit highly preferred orientation in the direction of the (111) plane. PZT nucleation is affected by two mechanisms:

(1) The lattice parameters of the intermetallic compound (Pt_3Ti) and Pt(111) match closely to PZT (111) [33, 34].

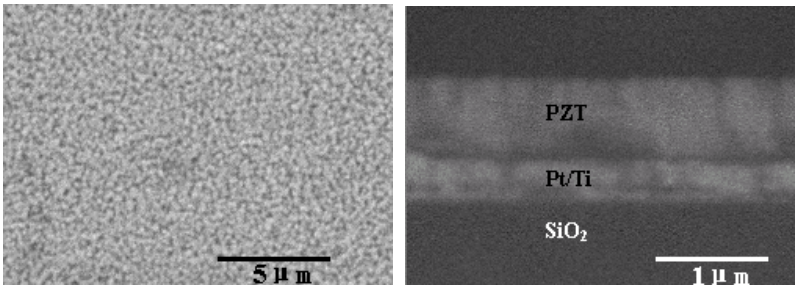

Figure 4. SEM surface and cross-section views of the films undergoing three annealing cycles (PZT-5*3).

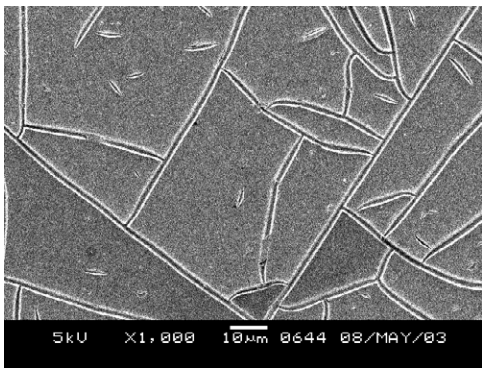

Figure 5. SEM surface view of the films undergoing four annealing cycles (PZT-5*4).

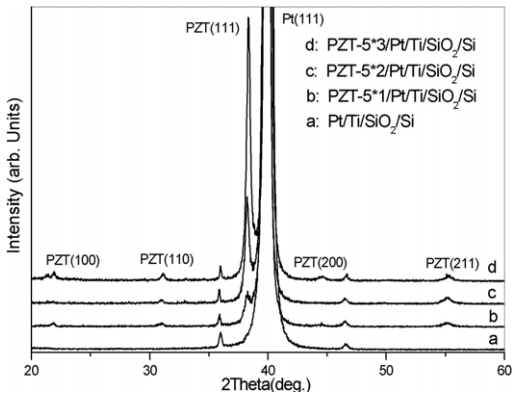

Figure 6. XRD patterns of $Pt/Ti/SiO_2/Si$ substrate (a) and PZT films with different thickness of (b) PZT-5*1, (c) PZT-5*2, and (d) PZT-5*3.

Therefore lattice matching is attributed to PZT(111) oriented growth.

(2) The (100) plane is the growth plane of the PZT with the lowest activation energy. Therefore, compared to the other oriented nuclei, the PZT(100) plane tends to grow more rapidly.

For the five-coating-layer-annealed process, the first mechanism governs the nucleation and growth of the PZT perovskite phase, thus PZT films show the (111) preferred orientation.

Figure 7 shows the XRD patterns of PZT films prepared by the one-coating-layer-annealed method. The PZT(100) peak shows a faster increase than PZT(111) peak with the film thickness. It is indicated that, for the films made with one-coating-layer-annealed process, the two mechanisms mentioned above affect PZT nucleation simultaneously. With the increase of the number of film coating layers, the effect of lattice matching between the substrate $Pt/Ti/SiO_2/Si$ and PZT films is suppressed by the mechanism of faster (100) plane growth with low activation energy. Therefore, the crystallites in the films show a tendency of transferring from approximately random (100) and (111) orientations of PZT-1*6 to the (100) preferred orientation of PZT-1*24. However, the PZT (100) peak has no increase with the film thickness for the five-layer-annealed process, as shown in figure 6. It is indicated that for the sol–gel method the coating layer in one annealing cycle plays an important role in the growth of the PZT(100) grains.

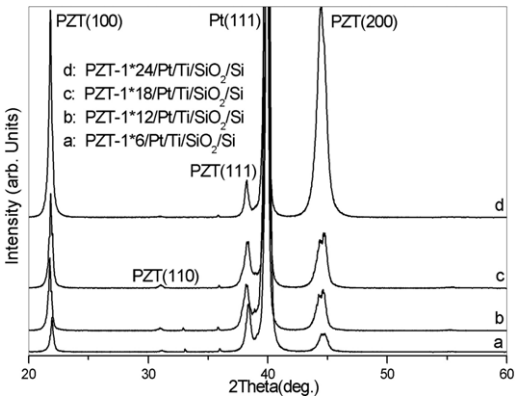

Figure 7. XRD patterns of PZT films with different thickness of (a) PZT-1*6, (b) PZT-1*12, (c) PZT-1*18 and (d) PZT-1*24.

3.4. Ferroelectric properties of the PZT films

Ferroelectricity was investigated by observing the polarization hysteresis loop, as shown in figure 8. For the PZT films prepared by both one-coating-layer-annealed and five-coating-layer-annealed methods, the remanent polarization (P_r) increases with the thickness of the PZT films, and little change is found in coercive fields (E_c). The ferroelectric properties of the PZT films are listed in table 1. It is indicated that good ferroelectric properties were obtained for one-coating-layer-annealed PZT films. Compared to PZT-5*3, these PZT films showed lower coercive fields.

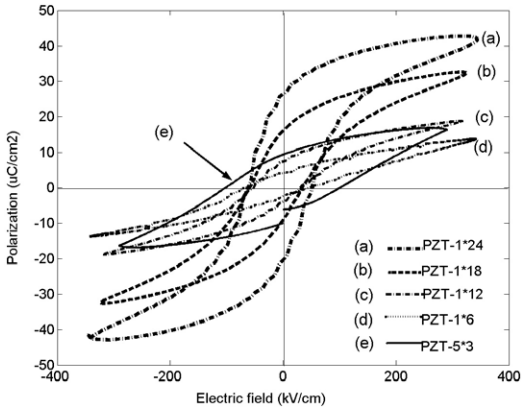

Figure 8. Ferroelectric hysteresis loops of PZT films of (a) PZT-1*24, (b) PZT-1*18, (c) PZT-1*12, (d) PZT-1*6, and (e) PZT-5*3.

Table 1. Ferroelectric properties of the PZT films prepared by one-coating-layer-annealed and five-coating-layer-annealed sol–gel methods.

Film type	Thickness (nm)	P_r (μC cm^{-2})	E_c (kV cm^{-1})
PZT-1*6	410	6.4	55.5
PZT-1*12	800	8.7	54.2
PZT-1*18	1200	18.9	54.0
PZT-1*24	1640	25.7	59.2
PZT-5*3	860	10.1	101.6

3.5. Fabrication of piezoelectric cantilever beams

Many groups have fabricated piezoelectric MEMS devices with one-layer PZT film using bulk micromachining techniques or surface micromachining techniques. Itoh *et al* [35] presented piezoelectric microcantilevers with bimorph sputtered ZnO films. Few reports have been found to integrate bimorph PZT films on silicon cantilever structures because of their high residual stress. We fabricated microcantilevers with bimorph or two-segment sol–gel PZT films using the wet and dry combined bulk micromachining techniques. The main advantage of this method is that an encapsulation layer is not needed to protect the PZT and electrode layers because the wet etching with KOH solution was carried out in the first step. The thickness of the cantilevers was accurately controlled by dry etching before freeing the microcantilevers.

Figure 9 shows the fabrication procedure of the bimorph PZT microcantilever. A 2 in diameter (100) n-type, double-side-polished silicon wafer (240 μm thickness) was prepared. 1.6 μm thermal oxide was grown on the wafer to serve as a mask layer for back-side silicon etching. The back-side silicon dioxide layer was patterned by wet etching (buffered hydrofluoric acid) to define the windows of silicon cups. Bulk silicon was anisotropically etched using KOH to make diaphragm structures with 60–80 μm thickness. Front-to-back-side alignment was done in second step. The front-side silicon dioxide layer was patterned to make front-side windows that will be used to free the cantilevers. A Pt/Ti (300 nm/100 nm) bottom electrode was deposited using an RF magnetron sputtering system and wet etched using aqua fortis. In step 3 the first PZT film (0.8 μm) with 12 coating layers was

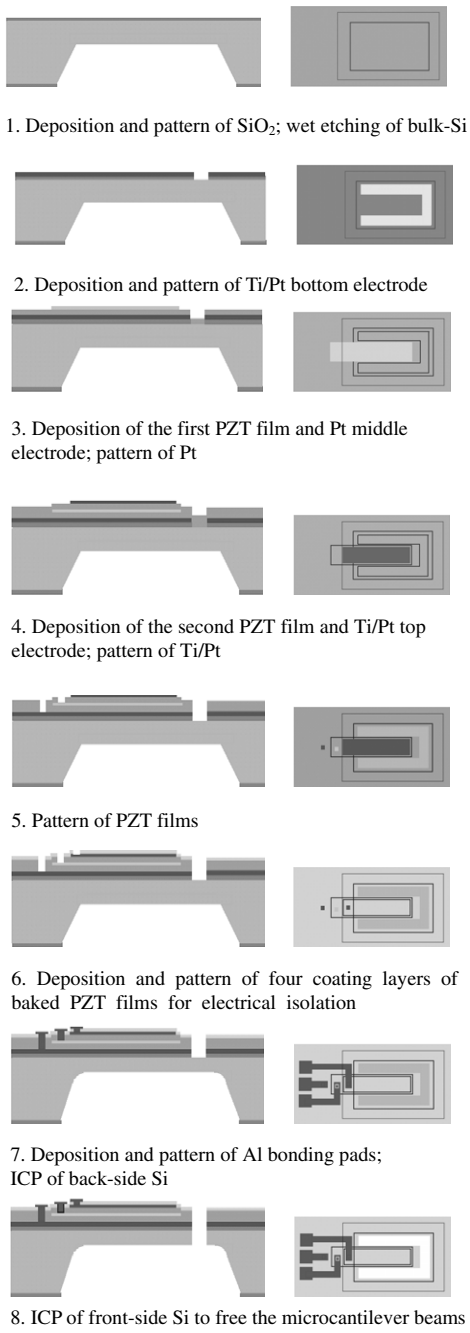

Figure 9. Fabrication procedure of bimorph PZT microcantilever.

prepared using the one-coating-layer-annealed sol–gel method. A Pt (80 nm) middle electrode was deposited and patterned using the lift-off technology. In this step, initial attempts at depositing a 20 nm Ti thin film to enhance the adhesion of the Pt film to the first PZT layer had been done. However, it is observed that, after the second PZT film was coated and annealed on the Pt/Ti middle electrode, the PZT/Pt/Ti layer peeled away from the first PZT layer. This phenomenon could in part be due to the reaction that occurs between the Ti layer and the first PZT layer during the high-temperature firing, but the mechanism that undermines the adhesion has not yet been identified. After this step, the second PZT film with 0.8 μm thickness was prepared using the same depositing process as

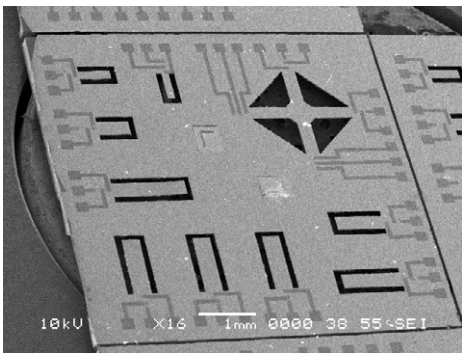

Figure 10. SEM micrograph of a micromachined piezoelectric MEMS cell.

the first PZT film. The Pt/Ti (80 nm/20 nm) top electrode was deposited and patterned by the lift-off technology. In step 5 the PZT films were patterned to make contact holes and front-side windows using HF:HCl:DI H_2O (1:30:70) for about 3 min. Then four coating layers of baked PZT films (total thickness of 260 nm) without post-annealing were deposited using the sol–gel method and patterned for electrical isolation. A layer of Al (340 nm) was deposited and patterned using the lift-off process to form the bonding pads. On the base of the wet etching, the back-side silicon was dry etched using an ICP (inductively coupled plasma) process to define the thickness of the microcantilevers. The final step was to use an ICP process to etch silicon in the front-side windows to free the PZT cantilevers.

(1) Deposition and pattern of SiO_2; wet etching of bulk-Si.
(2) Deposition and pattern of Ti/Pt bottom electrode.
(3) Deposition of the first PZT film and Pt middle electrode; pattern of Pt.
(4) Deposition of the second PZT film and Ti/Pt top electrode; pattern of Ti/Pt.
(5) Pattern of PZT films.
(6) Deposition and pattern of four coating layers of baked PZT films for electrical isolation.
(7) Deposition and pattern of Al bonding pads; ICP of back-side Si.
(8) ICP of front-side Si to free the microcantilever beams.

Different piezoelectric MEMS devices were designed on the same photomask set. Figure 10 shows an SEM micrograph of a micromachined piezoelectric MEMS cell, which includes six bimorph PZT cantilevers with various lengths and widths (540 μm $\times$ 130 μm, 540 μm $\times$ 180 μm, 540 μm $\times$ 280 μm, 840 μm $\times$ 280 μm, 1040 μm $\times$ 280 μm and 1240 μm $\times$ 280 μm), three two-segment PZT cantilevers with dimension of 1100 μm $\times$ 300 μm, and a four-end-fixed suspended structure. Each beam of the two-segment cantilevers and the four-end-fixed suspended structures includes one layer of piezoelectric film with two separated top electrodes. The proportion of the left-segment length to the right-segment length in the three two-segment cantilevers are 1:1, 1:2 and 2:1, respectively. The two piezoelectric parts in the bimorph and two-segment cantilevers serve as sensors, actuators, or a force sensor and an actuator, respectively. The four-end-fixed suspended structure is applied as a force sensor or an accelerometer. Figures 11(a) and (b) show the optical photographs of the micromachined bimorph and two-segment PZT cantilevers with dimensions of 1040 μm $\times$ 280 μm and 1100 μm $\times$ 300 μm. As shown in figure 11(b), the proportion of the left-segment length to the right-segment length of the two-segment PZT microcantilever is 1:1.

4. Conclusion

PZT thin films of various thickness were deposited on Pt(111)/Ti/SiO_2/Si(100) substrates by the sol–gel method. The baking and annealing temperatures were selected at 200 and 600 °C by analyzing the phase transformation of the PZT precursor solution. PZT films with (111) and (100) preferred orientation were obtained with the five-coating-layer-annealed and the one-coating-layer-annealed sol–gel methods, respectively. The coating layer in one annealing cycle affects both the growth of the PZT (100) grains and the residual stress of the PZT films. Compared to the five-coating-layer-annealed method, the one-coating-layer-annealed method apparently decreases the residual stress of the PZT films. The remanent polarization increases with the thickness of the PZT films. The P_r and E_c of the one-coating-layer-annealed PZT films with 1.6 μm thickness are 25.7 μC cm^{-2} and 59.2 kV cm^{-1}, respectively. PZT films prepared by the one-coating-layer-annealed method have lower coercive fields than five-coating-layer-annealed films. Two novel piezoelectric microcantilevers with two PZT piezoelectric elements (two layers or two segments of PZT films) and three electric electrodes were designed and fabricated with the wet and dry combined bulk micromachining techniques. As microsensors

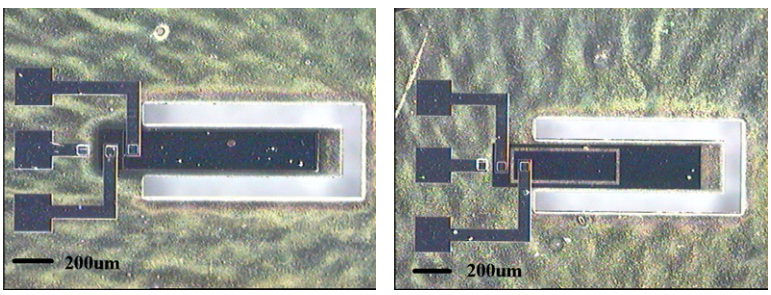

Figure 11. Optical photographs of micromachined bimorph (a) and two-segment (b) PZT microcantilevers.
(This figure is in colour only in the electronic version)

or microactuators, the bimorph piezoelectric cantilevers will increase the sensing resolution and actuation displacement (force) of the piezoelectric cantilevers. The bimorph and two-segment piezoelectric cantilevers can serve as a versatile device integrating sensing and actuating functions. The two piezoelectric elements can be used for the sensing and actuating elements, respectively. Force feedback and object manipulation will be realized simultaneously using the piezoelectric microcantilevers.

Acknowledgment

This work was supported by the National Natural Science Foundation of China (No. 90207003).

References

[1] Yamashita K *et al* 2002 Arrayed ultrasonic microsensors with high directivity for in-air use using PZT thin film on silicon diaphragms *Sensors Actuators* A **97/98** 302–7
[2] Lee C *et al* 1999 Self-excited piezoelectric PZT microcantilevers for dynamic SFM—with inherent sensing and actuating capabilities *Sensors Actuators* A **72** 179–88
[3] DeVoe D L and Pisano A P 2001 Surface micromachined piezoelectric accelerometers (PiXLs) *J. Microelectromech. Syst.* **10** 180–6
[4] Wang L-P, Wolf R A Jr, Wang Y, Deng K K, Zou L, Davis R J and Trolier-McKinstry S 2003 Design, fabrication, and measurement of high-sensitivity piezoelectric microelectromechanical systems accelerometers *J. Microelectromech. Syst.* **12** 433–9
[5] Luginbuhl Ph *et al* 1996 Piezoelectric cantilever beams actuated by PZT sol–gel thin film *Sensors Actuators* A **54** 530–5
[6] Kueppers H *et al* 2002 PZT thin films for piezoelectric microactuator applications *Sensors Actuators* A **97/98** 680–4
[7] Muralt P 2000 PZT thin films for microsensors and actuators: Where do we stand? *IEEE Trans. Ultrason. Ferroelectr. Freq. Control* **47** 903–15
[8] Luginbuhl Ph, Collins S D, Racine G-A, Grétillat M-A, De Rooij N F and Brooks K G 1998 Ultrasonic flexural Lamb-wave actuators based on PZT thin film *Sensors Actuators* A **64** 41–9
[9] Hong E, Krishnaswamy S V, Freidhoff C B and Trolier-McKinstry S 2005 Micromachined piezoelectric diaphragms actuated by ring shaped interdigitated transducer electrodes *Sensors Actuators* A **119** 521–7
[10] Shimizu M, Okaniwa M, Fujisawa H and Niu H 2004 Ferroelectric properties of Pb(Zr, Ti)O_3 thin films prepared by low-temperature MOCVD using $PbTiO_3$ seeds *J. Eur. Ceram. Soc.* **24** 1625–8
[11] Wang Z J, Chu J R, Maeda R and Kokawa H 2002 Effect of bottom electrodes on microstructures and electrical properties of sol–gel derived $Pb(Zr_{0.53}Ti_{0.47})O_3$ thin films *Thin Solid Films* **416** 66–71
[12] Cheng J and Meng Z 2001 Thickness-dependent microstructures and electrical properties of PZT films derived from sol–gel process *Thin Solid Films* **385** 5–10
[13] Lian L and Sottos N R 2000 Effects of thickness on the piezoelectric and dielectric properties of lead zirconate titanate thin films *J. Appl. Phys.* **87** 3941–9
[14] Lin C-H, Hsu W-D and Lin I-N 1999 Ferroelectric properties of $Pb(Zr_{0.52}Ti_{0.48})O_3$ thin films prepared by metal–organic decomposition process *Appl. Surf. Sci.* **142** 418–21
[15] Liqun D, Guiryong K, Fumihito A, Toshio F, Kouichi I and Yasunori T 2003 Structure design of micro touch sensor array *Sensors Actuators* A **107** 7–13
[16] Thomas R, Mochizuki S, Mihara T and Ishida T 2002 Effect of substrate temperature on the crystallization of Pb(Zr, Ti)O_3 films on Pt/Ti/Si substrates prepared by radio frequency magnetron sputtering with a stoichiometric oxide target *Mater. Sci. Eng.* B **95** 36–42
[17] Husmann A, Wesner D A, Schmidt J, Klotzbücher T, Mergens M and Kreutz E W 1997 Pulsed laser deposition of crystalline PZT thin films *Surf. Coat. Technol.* **97** 420–5
[18] Ledermann N *et al* 2003 {1 0 0}-textured, piezoelectric $Pb(Zr_x, Ti_{1-x})O_3$ thin films for MEMS: integration, deposition and properties *Sensors Actuators* A **105** 162–70
[19] Kim S-H, Park D-Y, Woo H-J, Lee D-S, Ha J, Hwang C S, Shim I-B and Kingon A I 2002 Orientation effects in chemical solution derived $Pb(Zr_{0.3}, Ti_{0.7})O_3$ thin films on ferroelectric properties *Thin Solid Films* **416** 264–70
[20] Lee J Y and Lee B S 2001 Orientation control and electrical properties of sputtered Pb(Zr, Ti)O_3 films *Mater. Sci. Eng.* B **79** 86–9
[21] Kim W S, Yang J-K and Park H-H 2001 Influence of preferred orientation of lead zirconate titanate thin film on the ferroelectric properties *Appl. Surf. Sci.* **169/170** 549–52
[22] Zhao M-H, Fu R, Lu D and Zhang T-Y 2002 Critical thickness for cracking of $Pb(Zr_{0.53}Ti_{0.47})O_3$ thin films deposited on Pt/Ti/Si(100) substrates *Acta Mater.* **50** 4241–54
[23] Muralt P, Kholkin A, Kohli M and Maeder T 1996 Piezoelectric actuation of PZT thin-film diaphragms at static and resonant conditions *Sensors Actuators* A **53** 398–404
[24] Muralt P 2000 Ferroelectric thin films for micro-sensors and actuators: a review *J. Micromech. Microeng.* **10** 136–46
[25] Kunz K, Enoksson P and Stemme G 2001 Highly sensitive triaxial silicon accelerometer with integrated PZT thin film detectors *Sensors Actuators* A **92** 156–60
[26] Kueppers H *et al* 2002 PZT thin films for piezoelectric microactuator applications *Sensors Actuators* A **97/98** 680–4
[27] Shibata T, Unno K, Makino E and Shimada S 2004 Fabrication and characterization of diamond AFM probe integrated with PZT thin film sensor and actuator *Sensors Actuators* A **114** 398–405
[28] Zurn S, Hsieh M, Smith G, Markus D, Zang M, Hughes G, Nam Y, Arik M and Polla D 2001 Fabrication and structural characterization of a resonant frequency PZT microcantilever *Smart Mater. Struct.* **10** 252–63
[29] Cui T *et al* 2004 Piezoelectric thin films formed by MOD on cantilever beams for micro sensors and actuators *Microsyst. Technol.* **10** 137–41
[30] Zhang Q Q, Gross S J, Tadigadapa S, Jackson T N, Djuth F T and Trolier-McKinstry S 2003 Lead zirconate titanate films for d_{33} mode cantilever actuators *Sensors Actuators* A **105** 91–7
[31] Itoh T and Suga T 1996 Self-excited force-sensing microcantilevers with piezoelectric thin films for dynamic scanning force microscopy *Sensors Actuators* A **54** 477–81
[32] Lee C and Itoh T 1999 Self-excited piezoelectric PZT microcantilevers for dynamic SFM—with inherent sensing and actuating capabilities *Sensors Actuators* A **72** 179–88
[33] Song Y J, Zhu Y and Desu S B 1998 Low temperature fabrication and properties of sol-gel derived (111) oriented $Pb(Zr_{1-x}Ti_x)O_3$ thin films *Appl. Phys. Lett.* **72** 2686–8
[34] Muralt P *et al* 1998 Texture control of $PbTiO_3$ and Pb(Zr, Ti)O_3 thin films with TiO_2 seeding *J. Appl. Phys.* **83** 3835–41
[35] Itoh T and Suga T 1996 Self-excited force-sensing microcantilevers with piezoelectric thin films for dynamic scanning force microscopy *Sensors Actuators* A **54** 477–81